View Article Online / Journal Homepage / Table of Contents for this issue
Dynamic Article Links

Nanoscale

Cite this: *Nanoscale*, 2012, **4**, 3168

www.rsc.org/nanoscale

PAPER

Nanoscale ear drum: Graphene based nanoscale sensors

Stas M. Avdoshenko,*[ab] Claudia Gomes da Rocha[ac] and Gianaurelio Cuniberti[a]

Received 12th January 2012, Accepted 11th March 2012
DOI: 10.1039/c2nr30097d

Published on 14 March 2012. Downloaded by University of Calgary on 11/29/2023 5:03:00 AM.

The difficulty in determining the mass of a sample increases as its size diminishes. At the nanoscale, there are no direct methods for resolving the mass of single molecules or nanoparticles and so more sophisticated approaches based on electromechanical phenomena are required. More importantly, one demands that such nanoelectromechanical techniques could provide not only information about the mass of the target molecules but also about their geometrical properties. In this sense, we report a theoretical study that illustrates in detail how graphene membranes can operate as nanoelectromechanical mass-sensor devices. Wide graphene sheets were exposed to different types and amounts of molecules and molecular dynamic simulations were employed to treat these doping processes statistically. We demonstrate that the mass variation effect and information about the graphene–molecule interactions can be inferred through dynamical response functions. Our results confirm the potential use of graphene as a mass detector device with remarkable precision in estimating variations in mass at the molecular scale and other physical properties of the dopants.

1 Introduction

The performance of nanoscale sensors is highly dependent on which material is used as the host object and its size. We can say that a promising detector should at least hold simultaneously optimal mechanical and electrical properties. An ideal candidate for such purposes is the one-atom-thick carbon layer known as graphene, the newest member of the "carbon allotrope family". Hailed as the thinnest and strongest material ever made, graphene has revolutionized the scientific frontiers in nanoscience and condensed matter Physics since its first isolation in 2004–2005.[1,2] Since then, a rich variety of remarkable physical features related to graphene structures has been reported, such as high carrier mobility,[3] almost perfect crystalline structure,[4] and an anomalous quantum Hall effect.[5]

Graphene has overcome the status of simply being an academic model for describing the properties of various carbon-based materials such as graphite, fullerenes and carbon nanotubes. The peculiar electronic and transport characteristics of graphene have guided researchers to explore several important physical phenomena where graphene appears as the main character in investigations focusing on spintronics,[6,7] ac/dc transport,[8,9] and thermoelectrics.[10–12] Additionally, graphene has fascinating mechanical properties such as lightness, flexibility, and robustness against breakage.[13] Such mechanical and electrical functionalities qualify graphene as an ideal candidate for fabricating nanoelectromechanical systems (NEMS).[14,15]

Recent experimental and theoretical studies have confirmed that the electronic response of graphene samples are rather sensitive to mechanical deformations.[16–18,20,21] Measurements coupling mechanical and electronic degrees of freedom in graphene include, for instance, a detailed analysis of band gap manipulation in uniaxially strained graphene membranes.[19,22] Pushing beyond the scope of electrical sensitivity to force, the holy grail of NEMS applications has been the implementation of nanoscale resonators capable of resolving the mass of single molecules or even single atoms. A new class of NEMS mass sensors was prompted with the design of carbon nanotube resonators anchored to an electrode surface.[23–25] Radio frequency waves are applied to the tube, inducing it to vibrate at a certain characteristic resonance frequency. The device can be exposed to other atoms or molecules that attach to the tube, and their presence as well as their mass can be detected through shifts in the resonant frequency. The same route was recently followed using monolayer graphene as resonators operating with electrical read-out and at room temperature.[26] Further understanding of the basic features of these devices, including their response with respect to applied voltage, the mass of foreign objects and temperature variations are required in order to boost graphene in nanoscale mass sensor applications. In this article, we illustrate how graphene membranes can serve as highly sensitive devices capable of measuring the mass and other properties of molecules adsorbed on their surface. Wide graphene sheets were exposed to different types and amounts of molecules and molecular dynamics simulations were employed to treat these doping processes statistically. Our results are in agreement with similar

[a]*Institute for Materials Science and Max Bergmann Center of Biomaterials Dresden University of Technology, D-01062 Dresden, Germany*
[b]*School of Materials Engineering, Purdue University, West Lafayette, Indiana, USA. E-mail: savdoshe@purdue.edu*
[c]*Nanoscience Center, University of Jyväskylä, 40014 Jyväskylä, Finland*

This journal is © The Royal Society of Chemistry 2012

View Article Online

Published on 14 March 2012. Downloaded by University of Calgary on 11/29/2023 5:03:00 AM.

ideas suggested by Russell and Král[27] in the understanding of the molecular configuration-sensitivity of graphene membranes. We demonstrate that the mass variation effect and information about the graphene–molecule interactions can be inferred through dynamical current-response functions and by means of the tunnelling current in a hypothetical (ac/dc)-NEMS device. Our results confirm the potential use of graphene-based detector devices with remarkable precision in estimating variations in mass at the molecular scale and other physical features of the dopants.

2 Methods

2.1 Molecular dynamics model

Our graphene membrane doped with three different molecules (fullerenes, coronenes and biphenyl) was treated *via* molecular dynamics (MD) simulations using the classical module FIRST embedded in the CP2k package.[28] The system's parameterization was written in the CHARMM[29] format based on the AMBER99[30] force field approximation using VEGAZZ[33] and home-made computational codes. The dynamical trajectories are described by a classical Lagrangian, $\mathscr{L}(\mathbf{r},\mathbf{p})$ with the isothermally constrained condition given by the Nosé–Hoover thermostat[36] applied to a system containing N particles. Classically, the bonded elements involve 2-, 3-, and 4-body interactions of covalently bonded atoms which account for the harmonic, angular and dihedral angular motions of the atoms, respectively. The non-bonded term is simply modelled *via* a long-range Lennard-Jones potential.

Overall, this formulation is classed as non-Hamiltonian, hence, an additional set of phase space coordinates, $\{\mathbf{s}, \dot{\mathbf{s}}\}$, is introduced in the description associated with an effective mass Q which determines the coupling between the reservoir and the system of interest. A dynamical average observable, A, can be computed following the NVT canonical ensemble where $\langle A(\mathbf{r},\mathbf{p}/s)\rangle_{\text{Nosé}} = \langle A(\mathbf{r},\mathbf{p}')\rangle_{\text{NVT}}$, with the scale factor $\text{L} = 3\text{N} + 1$ and $\mathbf{p}' = \mathbf{p}/s$ according to Nosé–Hoover.[36] A principal component analysis (PCA) was subsequently adopted to project the obtained dynamical trajectories onto a new uncorrelated basis set of vectors. The obtained MD trajectories were fitted to one reference value for calculating the variance–covariance matrixes of the interatomic fluctuations. The matrixes were diagonalized, leading to a set of uncorrelated harmonic distribution functions, corresponding to the principal components. The principal component (PC) modes were finally arranged in descending order with respect to their amplitudes and up to four components were selected for analysis. The PCA procedure was followed by using GROMACS[34] tools and the final data was visualized with the VMD[35] package.

2.2 Damped current calculation

The harmonic real space atomic translocations clearly visualized in our discussion led us to adopt a time-dependent continuous model to map the spectral current response of the pristine and doped graphene mat. It is worth mentioning that we are not interested in quantitative values for the current itself, but rather in the resonance frequency shifts caused by the presence of the molecules. Therefore, an effective transport model through a single channel perfectly suits our needs. Our first assumption is that the charges can ballistically flow through the graphene flake. The characteristic "wavy" shape of the membrane's vibrational modes clearly distinguishable after PCA treatment allow us to consider that our system obeys the same "mathematics" of a driven RLC circuit. To simulate such a harmonic charge flow through the system, the coupling between the graphene and the electrodes (τ) is considered to follow a harmonic dependency in time as $\tau \rightarrow \tau + \tau\sin(\omega t + \phi)$, with ω being the frequency of the mode and ϕ its dephasing angle. The analytical expression for the electronic transmission at a certain energy $\mathscr{E}$ of a single-level system [ε_0] attached to two symmetric electrodes can be written as

$$T(\mathscr{E}) = \frac{\tau^2}{(\mathscr{E} - \varepsilon_0 - \sigma)^2 + (\gamma/2)^2}. \quad (1)$$

The metallic leads are represented by the self-energy term $\Sigma = \sigma - i\gamma/2$ where its real part, σ, can shift the level up or down and its imaginary part, γ, accounts for the level broadening. Assuming a harmonic time-dependency for τ and using the Landauer–Bütticker equation, $I(\omega,t) = \int_{-\infty}^{+\infty} T(E',\omega,t)f(E')\mathrm{d}E'$ ($f(E')$ is the Fermi–Dirac distribution) we obtain

$$I(\omega,t) = I_0 + 2I_0\sin(\omega t + \phi) + O[(\ldots)^2] \quad (2)$$

where $I_0 = \int_{-\infty}^{+\infty} T(E)f(E)\mathrm{d}E$. Equation 2 is also a solution for the second order differential equation that describes the current flowing along an RLC driven circuit. Its solution written in terms of frequency is given by

$$|I(\omega)| \sim \frac{E}{\omega\alpha}\frac{1}{\sqrt{p^2+1}} \quad (3)$$

where $p = (\omega - \omega_{\text{ext}})/\alpha$, α is the attenuation parameter of the circuit, the dephasing angle is related to the frequency shift by $\tan(\phi) \sim 1/p$, and $\{\mathscr{E}, \omega_{\text{ext}}\}$ are the amplitude and the driving frequency, respectively, of an external pumping field expressed by $V(t) = E\cos(\omega_{\text{ext}}t)$.

3 Results and discussion

First, we introduce our system of study which is a graphene host membrane coupled to electrodes exposed to other molecules. Our results are interpreted based on the same physical principles applied to our ears; for example, one can estimate how large or far away a bouncing ball is only through the sound emitted when it hits the ground. Transferring this mechanism to our graphene based drum, we can say that graphene mimics the eardrum and the electrodes work as our neurons, transmitting the vibrations to the analyzer (the brain in this analogy). We demonstrate that it is possible to build a precise knowledge about the mass and other physical properties of the dopants by analyzing the signals coming from the systematic molecular collisions occurring between the molecules and the graphene membrane.

According to our computational protocol each system was explored with a 0.5 fs time step and a 20 ps total time under the classical force field approximation[30] parameterization created for aromatic carbon (sp^2 hybridization) and hydrogen atoms. All aromatic atoms are assumed to be neutral particles. The total time scale was chosen so as to be long enough to guarantee that quick atomic rearrangements were seen. Our mass sensor device

View Article Online

Published on 14 March 2012. Downloaded by University of Calgary on 11/29/2023 5:03:00 AM.

is idealized by a fully periodic graphene membrane vibrating at room temperature (T = 300 K) which is exposed to foreign organic molecules. The periodical graphene mat mimics the four point bounded sensor. As was reported, it is not optimal: Kim and Park have shown that it may suppress some edge-modes, which eventually leads to q-factor degradation.[20,21] At the same time, this constraint on the sensor geometry by the edge-mode reduction can eliminate the "edges variety problem". With a smaller impact from the edges, this can be advantageous from an experimental point of view. A classical Lagrangian with isothermal constraint conditions is given by the Nosé–Hoover thermostat:[36] the coupling time used in our calculations is 100 fs. The dimensions of the graphene flake are 60 × 60 Å^2, and as will be discussed further, the size of the detector dictates how precise the output of the sensor is. Three molecules with different affinities and topologies were chosen to interact with this membrane: (i) coronene (a flat macromolecule built from 6 attached benzene rings), (ii) biphenyl (two benzene rings tilted by 30° degrees) and (iii) fullerene (a hollow sphere molecule composed purely of carbon atoms). For the sake of simplicity, no explicit environments such as air or solvents were considered.

In Fig. 1, we show an example of the dynamics trajectories drawn by the molecules deposited on the graphene membrane at room temperature. The shadows capture a sequence of snapshots developed by the three systems of interest: the graphene flake interacting with four molecules of (a) coronene, (b) biphenyl and (c) fullerene, respectively. Each panel shows a representative trajectory of about 25 ps with 10 fs time sampling between frames. At a glance, one can clearly see that each molecule develops a different gliding route on the graphene plate. Coronene and biphenyl are rather mobile molecules leaving long tracking paths along the membrane. Buckyballs display slight dislocations on the graphene drum, bouncing mostly in the center of the drum. We can already infer that the geometrical shapes of the molecules will differently affect the vibrational movements of the graphene drum, offering an effective way to distinguish their physical features and mass.

To underline the real nature of the dynamical processes in our systems, we calculated the time-dependent velocity autocorrelation function (VAF), $C(t)$, which provides a mean value taken over the fluctuation regressions of all occurring initial velocities. Aspects related to the dynamical events can be observed in Fourier transforms of the VAF, which can unveil the intrinsically vibrational spectra of the molecular system. Additional information can be obtained by computing the classical dipole autocorrelation function (CDAF) in its spectral form. This

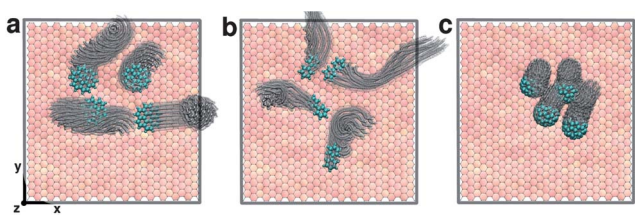

Fig. 1 Dynamic paths developed by four molecules of (a) coronene, (b) biphenyl and (c) fullerene added onto the graphene plate. Each snapshot which delineates the sequence of shadows completes a representative 25 ps trajectory with 10 fs sampling between frames.

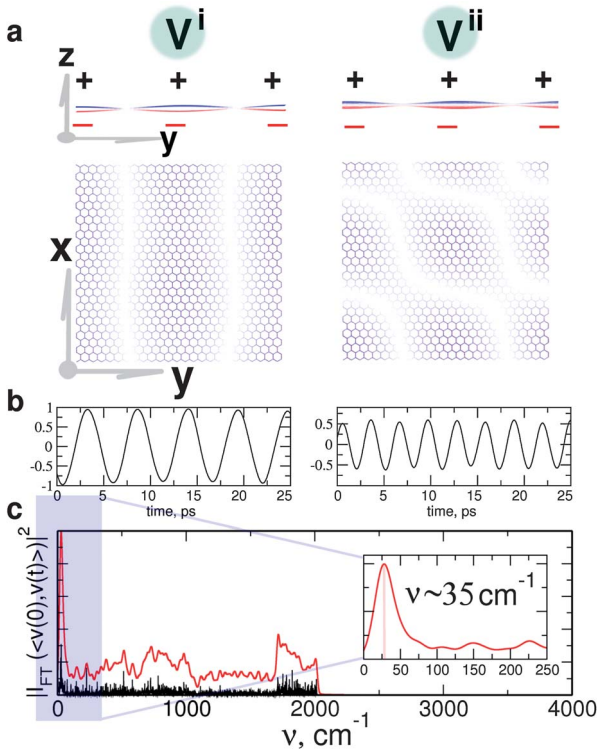

Fig. 2 Molecular dynamic results obtained for a pristine graphene plate. (a) First and second vibrational modes of a graphene membrane. Individual positive and negative displacements of the atoms with respect to the graphene plane are represented by + and − signals. (b) Trajectory projection on the two first principle component vectors labelled by V^i (left panel) and V^{ii} (right panel). (c) Vibrational density of states taken from the velocity autocorrelation function. The inset blows up the range of lower frequencies. Characteristic positive and negative atomic displacements shown in panel (a) are distinguished by red and black curves, respectively.

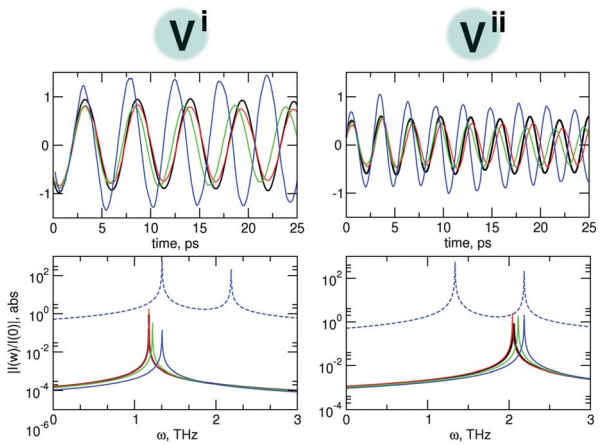

Fig. 3 (upper panel) Trajectory projections onto the first two principal component vectors (V^i and V^{ii}) for the graphene membrane in its pristine form (black) and doped with one (red), two (green), and four (blue) coronene molecules. (lower panel) Respective current curves [$I(\omega)/I(0)$] obtained from our harmonic model. The blue dashed line is the sum over the two components for the case where four molecules are added onto the graphene.

 This journal is © The Royal Society of Chemistry 2012

View Article Online

Published on 14 March 2012. Downloaded by University of Calgary on 11/29/2023 5:03:00 AM.

Table 1 Resonance frequency (ω_0), shift ($\delta\omega_0$) and molecular mass variation δm obtained for pristine graphene ("GR") and doped with coronene ("CR") or biphenyl ("BP") molecules

Structure	GR	+1 **CR**	+2 **CR**	+4 **CR**	+8 **CR**
ω_0/THz	1.176	1.179	1.220	1.337	1.200
$\delta\omega_0$/THz	0.000	0.003	0.044	0.161	[a]
δm/g mol^{-1}	—	43.0	**314.0**	575.0	[a]
Structure	**GR**	**+1 BP**	**+2 BP**	**+4 BP**	**+8 BP**
ω_0/THz	1.176	1.221	1.210	1.221	[a]
$\delta\omega_0$/THz	0.000	0.044	0.040	0.044	[a]
δm/g mol^{-1}	—	631.8	287.0	**158.0**	[a]

[a] These systems can not be mapped to a harmonic picture.

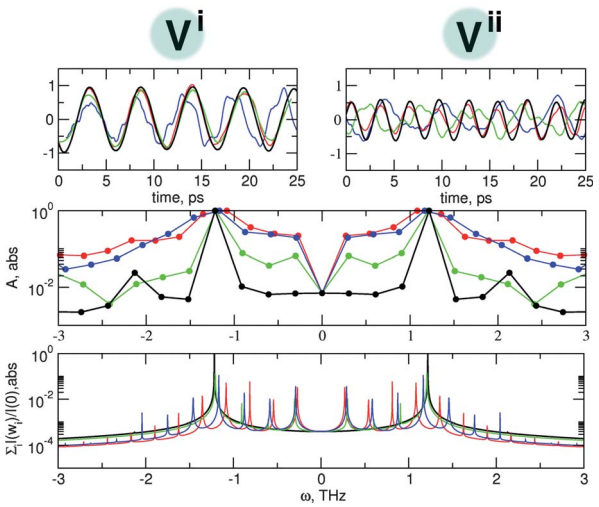

Fig. 4 (upper panel) Trajectory projections onto the two first principal component vectors (V^i and V^{ii}) for the pristine graphene layer (black) and the graphene layer doped with one (red), two (green), and four (blue) fullerene molecules. (middle panel) Spectral function taken from the trajectory projections performed over the first principal component vector. (lower panel) Current response behavior summed over all the harmonic modes extracted from eqn (3).

time-dependent autocorrelation function is defined as the Fourier transformation of the dipole moment autocorrelation function, $|d(t)|^2$, which is conceptually similar to infra-red (IR) spectral limits. The dynamical trajectories are then treated within principal component analysis (PCA) schemes, considerably simplifying the investigation of such complex physical phenomena.

Fig. 2(c) depicts the Fourier transformation of the VAF obtained firstly for our reference system, which is the pristine graphene membrane when no molecules are included. We split the spectral functions into two main contributions representing the positive (black curves) and negative (red curves) displacements of the atoms relative to the graphene plane. We also calculated the associated CDAF spectrum, which mimics the absorption line shape of fluctuating charges on the graphene layer under the influence of an incident electric field. We estimate high absorption intensities at the frequency $\sim$2000 cm^{-1}, which lies within the infra-red range. This frequency is about $\sim$400 cm^{-1} away from the experimental value obtained for graphite structures, but still it gives the correct expectation value for the

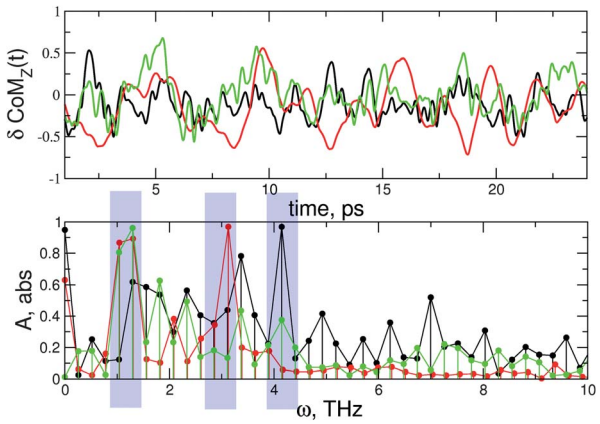

Fig. 5 (upper panel) Center of mass variation (δCoM) projected along the $\hat{z}$-component, which is perpendicular to the graphene plane as a function of time. (lower panel) Normalized Fourier transformation of the $\hat{z}$-component CoM deviation. The black, red and green curves correspond to the graphene membrane doped with coronene, fullerene, and biphenyl molecules, respectively.

maximum frequency window observed in the VAF spectrum. Additionally, the region of the VAF spectrum where most of its features appear ($\sim$1600 cm^{-1}) is in agreement with experimental measurements.

In addition, from the velocity spectral functions, one can identify in the inset of Fig. 2 a pronounced low frequency peak at the frequency of $\nu \approx 35$ cm^{-1}. This strong vibrational band corresponds to the fundamental frequency mode of the pristine graphene. By projecting the MD trajectory onto the two most significant principle vectors (V^i and V^{ii}), one can distinguish between these main oscillatory modes. The period of the first fundamental mode (V^i) is given by $\sim$6 ps and its equivalent frequency corresponds exactly to the value of $\nu = 35$ cm^{-1}, which is also observed in the VAF spectral function. The second mode was also calculated by characterizing the second highest transversal displacements of the graphene membrane with respect to its plane. Such real space characteristics of atomic translocations regarding the first two principal component (PC) vectors are well illustrated on panel (a) of Fig. 2. Regular oscillation patterns can be seen, indicating that the graphene layer apparently behaves as a continuous membrane. It is also straightforward to assume that such PC modes are related to the membrane tension. In this sense, we expect that these two principal components will be significantly disturbed as molecules are placed on the membrane surface. Although in principle a continuum description could work as a first approximation, we will proceed with our investigation by probing dynamically the sensitivity of the device through a complete atomistic representation.

After analyzing in detail the dynamic response of a pristine graphene mat, we are able to identify how these modes are affected by the inclusion of other molecules. As a first example, we consider an isotopic condition where we keep the same type of molecule (coronene) while changing the amount that is adsorbed onto the graphene. Fig. 3 (upper panels) reveals the trajectory projections on the two first principle component vectors for up to four coronene molecules doping the graphene layer. The red, green and blue curves correspond to situations where one, two, and four molecules stand on the graphene sheet, respectively.

View Article Online

Published on 14 March 2012. Downloaded by University of Calgary on 11/29/2023 5:03:00 AM.

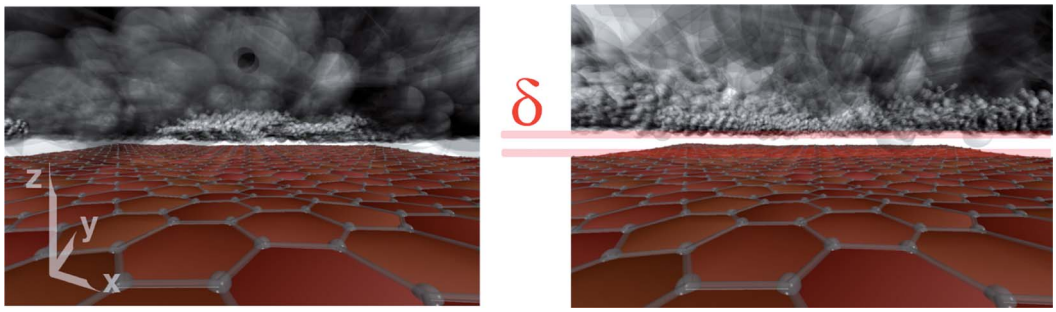

Fig. 6 Planar view of the trajectory clouds drawn by the four coronene and biphenyl molecules on the membrane. δ shows the more pronounced separation between biphenyl objects and the graphene.

One can clearly see that the curves undergo shifts as more molecules interact with the graphene, indicating that the natural vibrations of the membrane are disturbed in response to changes in the environment. For a better visualization of such shifts, we converted the time-dependent projections into current spectral functions by assuming that our doped graphene membrane behaves as a single-level transmission system. Based on the regular oscillatory patterns seen in Fig. 2(a), we represent the graphene detector as an RLC circuit operating at a characteristic resonance frequency of ω_0. We adapted the differential equation of a driven harmonic circuit to our system, where a time dependent power source, $V(t) = E\cos(\omega_{ext}t)$, pumping charges with a frequency of ω_{ext} will scan the resonance frequency of the pristine and doped structures in the ballistic regime. The solution for a RLC system written in terms of frequency is given by

$$|I(\omega_0)| \sim \frac{E}{\omega_0\alpha}\frac{1}{\sqrt{p^2+1}} \quad (4)$$

where E is the oscillation amplitude of the driven field, α is the attenuation parameter, and $\rho = (\omega_0 - \omega_{ext})\alpha$.

The estimated current spectral functions are shown on the lower panels of Fig. 3 using the resonance frequencies taken from the PC plots and an attenuation of $\alpha = 1.0$ THz. The same color legend used on the upper panels of Fig. 3 is adopted to represent the situations where up to four coronene molecules dope the graphene drum. The dashed lines show the sum over the two components when four molecules stick to the graphene sheet. Looking initially at the current profiles for each component representing the pure graphene membrane, resonance peaks at ~1.17 THz and ~2.10 THz are found. As more coronene molecules are placed on the membrane, the peaks gradually move upwards in frequency.

In standard MEMS devices the mass loading usually does not affect the mechanical tension of the sensor and so one can say the fundamental frequency of the oscillator changes in terms of mass as $\delta\omega_0 = -\delta m_{eff}\omega_0 2m$, where m_{eff} and m are the effective mass of the whole doped and pristine membrane, respectively.[26] As a first approximation, we follow this simple interpretation to compute the results shown in Table 1, which shows the estimated values for the first PC resonance mode ω_0, its frequency shift $\delta\omega_0$ as more molecules are loaded, and the associated mass variation δm per molecule. One, two, four and eight molecules of coronene ("CR") and biphenyl ("BP") attach onto the graphene drum ("GR"). It is important to point out here that the so-called MEMS formula above for the harmonic strain has a limit based on the mass ratio $\delta m/m_{dev} \sim 0.01$ (δm is the loaded mass and m_{dev} is the device mass) according to Dohn *et al.*,[31] although some variations are possible.[32] For all our systems with single molecules, harmonic mapping is valid for values of $\delta m/m_{dev} < 0.015$. In our work, we were guided more by the PCA vector changes in making a decision on the adequacy of the harmonic interpretation.

Also, in such atomically thin resonators, the interaction between the mat and the dopant plays an important role in its response since the loading mass can interfere with the intrinsic tension of the sensor. In reality, the adsorbates can impart extra tension to the membrane, thus promoting an upward frequency shift, as shown by our results. This also raises an important point regarding the use of graphene as NEMS. Since graphene's interaction with foreign objects is an issue here, its functional detecting area is a prominent parameter that must be carefully adjusted in order to achieve optimal sensory performances. Such peculiar detection features could only be observed when one considers a full atomistic description of the system, such as the one used here, instead of a phenomenological continuous model.

Discussing in more detail the results displayed in Table 1, we can see that the first resonance mode for coronene doping gradually moves to higher frequency ranges as more molecules are included, but it shifts back when 8 molecules are added. From the simulations it is possible to see that 8 coronene molecules cover a considerable area of the graphene membrane, characterizing a limit that we name "full coating". Therefore, such an number of coronene flat objects restrains some of the natural vibrations of the graphene. In other words, additional nodal lines are imparted on the doped graphene membrane due to the presence of the relatively large coronene molecules. Adopting our harmonic expectation for the frequency–mass variation proportion, an excellent agreement with the real molar mass of coronene molecules (300.35 g mol^{-1}) is obtained when the graphene host receives two dopants. We have thus identified a situation where the resonator is capable of providing a precise mass response. In this case, a 60 × 60 $Å^2$ graphene membrane doped with two adsorbed coronene molecules comprises the optimum ratio between the functional area of the sensor and the amount of dopant.

The example of single coronene doping is also a state where the sensor is still not able to provide a good measurement, and we identify this as a "diluted regime". Firstly, the graphene membrane is still rather relaxed due to the low quantity of molecules. As a result, the membrane can only capture most of

 This journal is © The Royal Society of Chemistry 2012

View Article Online

Published on 14 March 2012. Downloaded by University of Calgary on 11/29/2023 5:03:00 AM.

the thermal vibrations of the molecule. Secondly, the coronene molecules present a regular flat topology which causes a rather weak effect on the graphene under single doping. Two molecules could then induce the perfect signal on the sensor. In contrast to coronene dopants, biphenyl (BP) objects already induce an abrupt shift in frequency in the single doping case, until it saturates at around 0.04 THz no matter how many molecules are loaded. Such small fluctuations in frequency as the sensor is loaded with impurities indicates a weak interaction between the biphenyl and the graphene.

The erratic shape of a single biphenyl compound yields strong and long dynamical movements along the graphene drum, as demonstrated in Fig. 1, but this is even more evident for single doping. This can give the sensor device the "wrong impression" that a large number of molecules are bouncing on it. For this reason, the presence of a single biphenyl molecule prompted a high mass variation on the system of 631.0 g mol^{-1}. As more biphenyl molecules are included on the sensor, the direct interaction between them starts to restrain their dynamical trajectories. Their repulsion exerts a significant constraint on their kinetic vibrations, allowing the graphene detector to perceive their mass more efficiently. The situation with four adsorbed molecules retains the best molar mass estimation of 158.0 g mol^{-1} per molecule, in comparison to its real value of 154.21 g mol^{-1}. Once more, we detected the optimum (sensor area) : (amount of impurities) ratio in which the device can provide accurate responses. Eventually, a "full coating" state is reached as more molecules bounce on the graphene mat, and again the sensor responds inaccurately.

In Fig. 4 we present the results obtained for our third example system; fullerene. Fullerene doping brings a situation where the sensor is not able to give any mass output. This is due to the fact that this system deviates from harmonic behavior. This can be seen on the upper panels of Fig. 4 showing the trajectory projections onto the two first principal components for the pristine graphene (black curve) and the graphene doped with one (red curve), two (green curve), and four (blue curve) buckyballs. For the second principal component solution in particular, the characteristic sinusoidal shape of the projections is severely disturbed. Therefore, a mass detection device based on $\delta\omega_0/\delta m_{\mathrm{eff}}$ proportionality is not effective since it is not possible to decompose the harmonic modes of the PC projections. The complete signal of the sensor in response to fullerene doping can still be mapped onto current spectral functions containing all the available modes, which is shown in the lower panels of Fig. 4.

So far, we have demonstrated that the size of the detection area with respect to the type of dopant matters in the case of implementing graphene membranes as nanosensor systems. In contrast to estimations obtained by continuous models, the full atomistic description reveals that graphene mats that are too small can fail in sensing the mass of the molecules. A similar size dilemma has also been observed experimentally.[26] Nonetheless, the abilities of such membranes should not be underestimated since they are not limited to mass detection. As long as a proper dynamic formulation is followed, it is possible to verify that these materials can infer other properties of the adsorbed molecules and their interaction with the detector. We based this on the idea that the molecules can imprint their "identity" on the membrane over time. The signature of the molecule can be read by calculating the molecular center of mass (CoM) motion and its statistical correlation.

Fig. 5 (upper panel) presents the evolution over time of deviations in the center of mass (δCoM) along the z-direction (perpendicular to the graphene plane) for each doping molecule. The lower panel shows their respective Fourier transformations, which can be interpreted as the "sound" emitted by each particular dopant and how the graphene is codifying them. The well-defined circular shape of the fullerenes results in a rather smooth dependency of its CoM on time. It oscillates almost uniformly and with large amplitudes, indicating that buckyballs mostly bounce on top of the graphene in a repetitive way. This limited bouncing movement leads to the relatively narrow spectral response of its CoM deviation, with most of its signal being below 4.0 THz. The coronene molecules exhibit noisier behaviour in their CoM variation, though it fluctuates around small amplitudes during most of its dynamic trajectory. Its spectral function is richer in comparison to the fullerene example, with sharp signals popping up along the entire frequency range. Its highest responses are slightly "blue-shifted", being located inside the frequency window of 0.0–4.3 THz. Our last example, the biphenyl molecule, is significantly more noisy, with dynamical fluctuations reaching high amplitudes. Its spectral response shows relevant signals up to 4.8 THz, followed by a short suppression between 4.8–6.0 THz, as for fullerene. For some reason, fullerene and biphenyl cannot be "heard" by the graphene at this frequency range. Above 6.0 THz the signal of biphenyl is recovered.

For a better illustration of such imprints, we show in Fig. 6 a planar view of the dynamic trajectories already presented in Fig. 1 drawn by four coronene (left panel) and biphenyl (right panel) molecules. The dynamic on-the-fly path of the coronene molecules reveals that they stand closer to the membrane, in contrast to the biphenyl, which is mostly repelled from the membrane. Such information about the interaction with the detector and the shape of the molecules were successfully captured by the CoM curves. As discussed previously, biphenyl with its twisted benzene rings triggers intense kinetic movements on the graphene mat. As a consequence, the molecules move away from the membrane and their CoM deviation undergoes strong dynamical fluctuations. Coronene expresses its flat form in terms of a noisy CoM, but it vibrates within low amplitudes. Finally, the buckyball and its characteristic bouncing movement on the graphene surface is evident through its extended oscillatory behaviour of the CoM. In addition, the three molecules reveal their most intense CoM signals at clearly distinguishable frequencies: 3.2 THz (fullerene), 4.1 THz (coronene), and 1.2 THz (biphenyl). These results confirm that each molecule can imprint a sort of "identification" on the graphene ear.

4 Conclusions

In summary, our work underlines the possibility of using a graphene membrane as a nanoscale detector. We developed a complete theoretical framework based on classical molecular dynamics assumptions and elaborated a statistical analysis of the time-dependent trajectories subsequently mapped onto spectral current curves. Our results point out that such classical approximations for the molecule–membrane pairs is enough to

View Article Online

Published on 14 March 2012. Downloaded by University of Calgary on 11/29/2023 5:03:00 AM.

demonstrate the promising sensing abilities of the device, which can resolve molecules with closely related properties. At first glance, one might say that the performance of our graphene-based device is inferior in comparison to specifically oriented mass spectrometers. Nevertheless, what our calculations really demonstrate is that graphene membranes are able to measure effectively the mass of adsorbed dopants for intermediate levels of coverage of the graphene drum. In other words, the interplay between the size of the membrane and the concentration of the analyte can play a crucial role in their performance. We also show that it is feasible to detect specific "fingerprints" left by the molecules on the graphene mat and they can be inferred by IR or even Raman spectroscopy. Depending on the shape of the molecule, distinct signals can be captured by the graphene flake as a result of the dynamical movements generated by the dopants on its surface. We expect that several technological branches, particularly in the NEMS industry, could benefit from our graphene-based drum: a nanoscale "ear" that can hear the "sounds" produced by other molecules.

Acknowledgements

CGR would like to thank the Alexander von Humboldt Foundation. SMA is thankful for financial support from the Erasmus Mundus programme External Co-operation (EM ECW-L04 TUD 08-11).

References

1 K. S. Novoselov, A. K. Geim, S. V. Morozov, D. Jiang, Y. Zhang, S. V. Dubonos, I. V. Grigorieva and A. A. Firsov, *Science*, 2004, **306**, 666.
2 K. S. Novoselov, A. K. Geim, S. V. Morozov, D. Jiang, M. I. Katsnelson, I. V. Grigorieva, S. V. Dubonos and A. A. Firsov, *Nature*, 2005, **438**, 197–200.
3 Y. W. Tan, Y. Zhang, K. Bolotin, Y. Zhao, S. Adam, E. H. Hwang, S. Das Sarma, H. L. Stormer and P. Kim, *Phys. Rev. Lett.*, 2007, **99**, 246803.
4 C. H. Lui, L. Liu, K. F. Mak, G. W. Flynn and T. F. Heinz, *Nature*, 2009, **462**, 339–341.
5 K. S. Novoselov, Z. Jiang, Y. Zhang, S. V. Morozov, H. L. Stormer, U. Zeitler, J. C. Maan, G. S. Boebinger, P. Kim and A. K. Geim, *Science*, 2007, **315**, 1379.
6 J. Kunstmann, C. zdogan, A. Quandt and H. Fehsk, *Phys. Rev. B: Condens. Matter Mater. Phys.*, 2011, **83**, 045414.
7 F. S. M. Guimaraes, A. T. Costa, R. B. Muniz and M. S. Ferreira, *Phys. Rev. B: Condens. Matter Mater. Phys.*, 2010, **81**, 233402.
8 C. G. Rocha, L. E. F. Foa Torres and G. Cuniberti, *Phys. Rev. B: Condens. Matter Mater. Phys.*, 2010, **81**, 115435.
9 C. Ritter, S. S. Makler and A. Latge, *Phys. Rev. B: Condens. Matter Mater. Phys.*, 2008, **77**, 195443.
10 N. Mingo, K. Esfarjani, D. A. Broido and D. A. Stewart, *Phys. Rev. B: Condens. Matter Mater. Phys.*, 2010, **81**, 045408.
11 H. Sevincli and G. Cuniberti, *Phys. Rev. B: Condens. Matter Mater. Phys.*, 2010, **81**, 113401.
12 A. D. Liao, J. Z. Wu, X. Wang, K. Tahy, D. Jena, H. Dai and E. Pop, *Phys. Rev. Lett.*, 2011, **106**, 256801.
13 I. W. Frank, D. M. Tanenbaum, A. M. van der Zande and P. L. McEuen, *J. Vac. Sci. Technol., B: Microelectron. Nanometer Struct.–Process., Meas., Phenom.*, 2007, **25**, 2558.
14 A. K. Httel, G. A. Steele, B. Witkamp, M. Poot, L. P. Kouwenhoven and Herre S. J. van der Zant, *Nano Lett.*, 2009, **9**, 2547.
15 D. Garcia-Sanchez, A. M. van der Zande, A. San Paulo, B. Lassagne, P. L. McEuen and A. Bachtold, *Nano Lett.*, 2008, **8**, 1399.
16 T. M. G. Mohiuddin, A. Lombardo, R. R. Nair, A. Bonetti, G. Savini, R. Jalil, N. Bonini, D. M. Basko, C. Galiotis, N. Marzari, K. S. Novoselov, A. K. Geim and A. C. Ferrari, *Phys. Rev. B: Condens. Matter Mater. Phys.*, 2009, **79**, 205433.
17 M. Poetschke, C. G. Rocha, L. E. F. Foa Torres, S. Roche and G. Cuniberti, *Phys. Rev. B: Condens. Matter Mater. Phys.*, 2010, **81**, 193404.
18 V. M. Pereira, N. M. R. Peres and A. H. Castro Neto, *Phys. Rev. B: Condens. Matter Mater. Phys.*, 2009, **80**, 045401.
19 J. S. Bunch, A. M. van der Zande, S. S. Verbridge, I. W. Frank, D. M. Tanenbaum, J. M. Parpia, H. G. Craighead and P. L. McEuen, *Science*, 2007, **315**, 490.
20 S. Y. Kim and H. S. Park, *Nano Lett.*, 2009, **9**, 969–974.
21 S. Y. Kim and H. S. Park, *Nanotechnology*, 2010, 21.
22 J. T. Robinson, M. Zalalutdinov, J. W. Baldwin, E. S. Snow, Z. Wei, P. Sheehan and B. H. Houston, *Nano Lett.*, 2008, **8**, 3441.
23 R. Mateiu, Z. J. Davis, D. N. Madsen, K. Molhave, P. Boggild, A. M. Rassmusen, M. Brorson, C. J. H. Jacobsen and A. Boisen, *Microelectron. Eng.*, 2004, **73–74**, 670–674.
24 B. Lassagne, D. Garcia-Sanchez, A. Aguasca and A. Bachtold, *Nano Lett.*, 2008, **8**, 3735–3738.
25 Y. Li, X. Qiu, F. Yang, X.-S. Wang and Y. Yin, *Nanotechnology*, 2008, **19**, 165502.
26 C. Chen, S. Rosenblatt, K. I. Bolotin, W. Kalb, P. Kim, I. Kymissis, H. L. Stormer, T. F. Heinz and J. Hone, *Nat. Nanotechnol.*, 2009, **4**, 861–867.
27 J. Russell and P. Král, Configuration-sensitive Molecular Sensing on Doped Graphene Sheets, *Nano Res.*, 2010, **3**, 472.
28 The CP2K developers group (2010), http://cp2k.berlios.de.
29 B. R. Brooks, *et al.*, *J. Comput. Chem.*, 1983, **4**, 187–217.
30 J. Wang, R. M. Wolf, J. W. Caldwell, P. A. Kollman and D. A. Case, *J. Comput. Chem.*, 2004, **25**, 1157–1174.
31 S. Dohn, W. Svendsen, A. Boisen and O. Hansen, *Rev. Sci. Instrum.*, 2007, **78**, 103303.
32 S. Schmid, S. Dohn and A. Boisen, *Sensors*, 2010, **10**, 8092–8100.
33 A. Pedretti, L. Villa and G. Vistoli, *J. Mol. Graphics Modell.*, 2002, **21**, 47–49.
34 E. Lindahl, B. Hess and D. van der Spoel, *J. Mol. Mod.*, 2001, **7**, 306–317.
35 W. Humphrey, A. Dalke and K. Schulte, *J. Mol. Graphics*, 1996, **14**, 33–38.
36 W. G. Hoover, *Phys. Rev. A: At., Mol., Opt. Phys.*, 1985, **31**, 1695.

 This journal is © The Royal Society of Chemistry 2012